Field Measurement and Finite Element Simulation of the Impacts of Reduced Truck Tire Pressure on Strain Response

Qingfan Liu, PhD Candidate
Department of Civil Engineering
University of Manitoba
umliu277@cc.umanitoba.ca

Ahmed Shalaby, Ph.D., P.Eng.
Professor of Civil Engineering
University of Manitoba
shalabya@cc.umanitoba.ca

Paper prepared for presentation
at the *Challenges Facing Low-volume Roads* Session
of the 2011 Annual Conference of the
Transportation Association of Canada
Edmonton, Alberta

ABSTRACT

The reduced tire pressure could lower the tire-pavement contact stresses and the associated damage to the pavement. A study was carried out by the University of Manitoba to evaluate the effects of reduced tire pressure, in lieu of reduced loads, during the spring thaw period. Asphalt strain gauges were installed in a section of a low volume haul road in central Manitoba. Field testing was conducted in the spring using an 8-axle double semi-trailer equipped with a semi-automated tire pressure control system. The tests were conducted at various loads, truck speeds, and at the normal and reduced tire pressures.

The results of the field testing showed that when tire pressure was reduced by fifty percent, the normalized measured tensile strain at the bottom of asphalt layer was reduced by an average of 15%. The effects of the direction of strain, truck speed, and tire offset from the strain gauge were analyzed and presented.

A 3-dimension finite element model was developed to simulate the pavement responses to normal and reduced truck tire pressure. The modeling results were verified by field data. The results from both field data and simulation indicated that the tire pressure control system is effective to prevent bottom up failure of the pavement.

1. INTRODUCTION

Tire pressure control system (TPCS) would provide considerable benefits to both the road agency and the road user in the form of lower costs for construction and maintenance (1).

From 2000 to 2003, the Forest Engineering Research Institute of Canada (FERIC) conducted full-scale tests on a variety of thin pavements in British Columbia, Canada based on their modeling process. During those tests, fully loaded log trucks were able to haul during the last 3 to 5 weeks of the spring load restriction period with no measureable increase in pavement rutting or cracking(2).

Strain gauges were installed at the bottom of asphalt concrete (AC) underneath the outer wheel path in a section of provincial truck highway PTH11 in Manitoba. The resilient moduli of various layers were back-calculated from falling weight deflectometer deflections using ELMOD software. Pavement structures and back-calculated layer moduli are shown in Table 1.

Table 1 Pavement Structures and Back-Calculated Layer Moduli

Layer	Thickness (mm)	Back-Calculated Moduli (MPa)	Poisson's Ratio
AC	130	2,700	0.35
Base	335	250	0.40
Clay subgrade	--	35	0.45

2. FIELD TESTS

To evaluate the effects of reduced tire pressure for low volume roads, a series of TPCS tests were carried out at the instrumented test section in spring 2009. The variables were as follows:

- Three axle configurations: tandem drive axle, tridem trailer1 axle, and tandem trailer2 axle.
- Two tire load levels: 1930 kg or 2173 kg equivalent to Manitoba classification for A1 normal (A1N) and Roads and Transportation Association of Canada (RTAC) normal unrestricted load respectively.
- Two tire pressures: 345 kPa and 690 kPa
- Two truck speeds: 20 km/h and 70km/h.

Strains of the installed strain gauges were collected when the test truck passed the instrumented section. An example of strain response at the bottom of AC layer and tire groups of the test truck is shown in Figure 1.

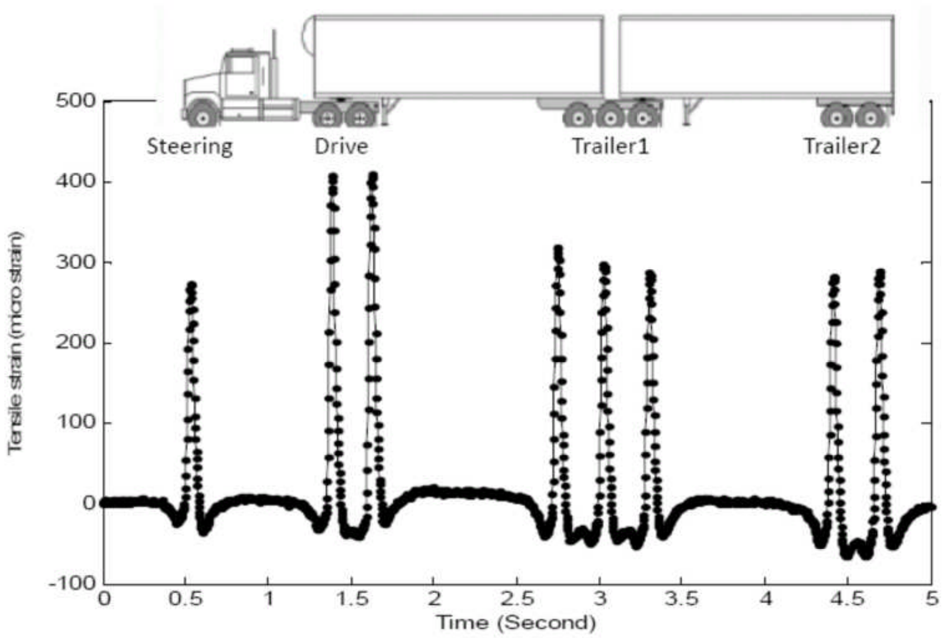

Figure 1 An example of strain response and tire groups.

2.1 Footprints and Wheel Offset

The non-uniform tire contact stress distributions were measured in field right before field test using an I-Scan contact pressure mat made by Tekscan Pressurement System Inc. Tire and axle load were also checked using a portable scale. Figure 2 shows graphically two typical footprints under A1N load at the tire pressure of 690 kPa and 345 kPa, respectively.

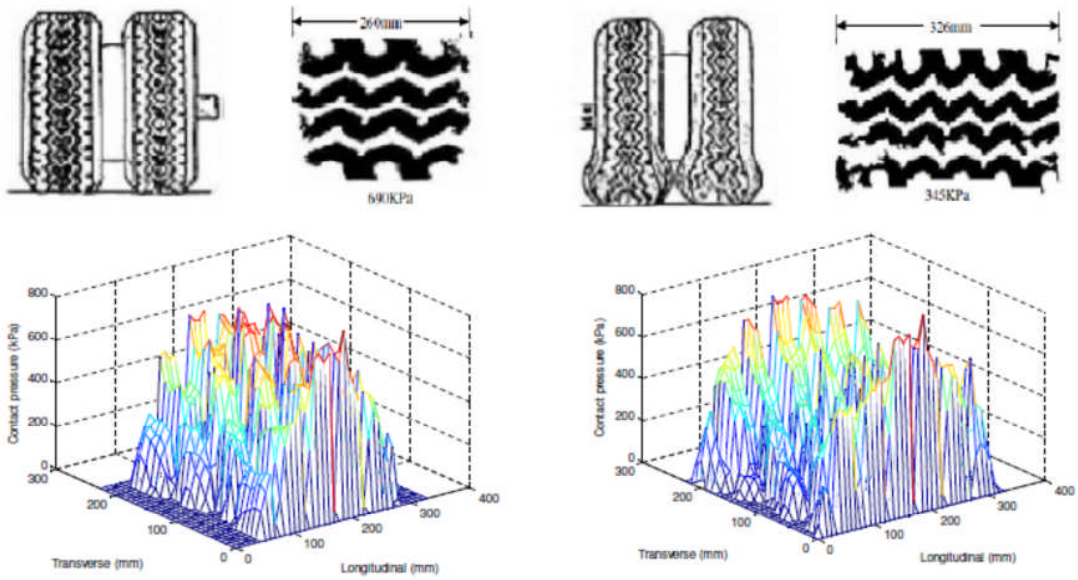

Figure 2 Measured footprints at 690 kPa (left) and 345 kPa (right) with A1N load.

Table 2 shows the area of footprint and the increase when tire pressure deflated from 690 kPa to 345 kPa for various loads and axles.

Table 2 Footprint areas and Their Increase when Tire Pressure Deflated from 690kPa to 345 kPa

Load rating	Measured tire load (kg)	Tire footprint area for 690 kPa (mm^2)	Tire footprint area for 345 kPa (mm^2)	Footprint area difference (%) from 690 kPa to 345 kPa
A1N	1930	48337	58244	17
RTAC	2173	47916	59087	19

A video camera was set up to monitor the track of the test truck. Wheel offset of each tire group is available by reviewing the video footage of each run.

2.2 Statistical Analysis of Field Data

A linear regression model was developed to determine the relationship between the measured strains and tire offsets. The linear relationship for this analysis is valid only for offsets less than 200 mm. For the cases where larger wheel offsets were encountered, the relationship was non-linear and similar to Timm and Priest (3) approximation of a second order polynomial for offsets from 0-1000 mm. Figure 3 and Figure 4 show the plot of measured transverse and longitudinal strains versus tire offset for two test loads at 20 km/h and 345 kPa tire pressure. The measured strains can be normalized to zero offset by using the following equation:

$$\textit{Normalized strain} = \textit{measured strain} + \beta \times \textit{offset}$$

Where: β is the slope of regression line.

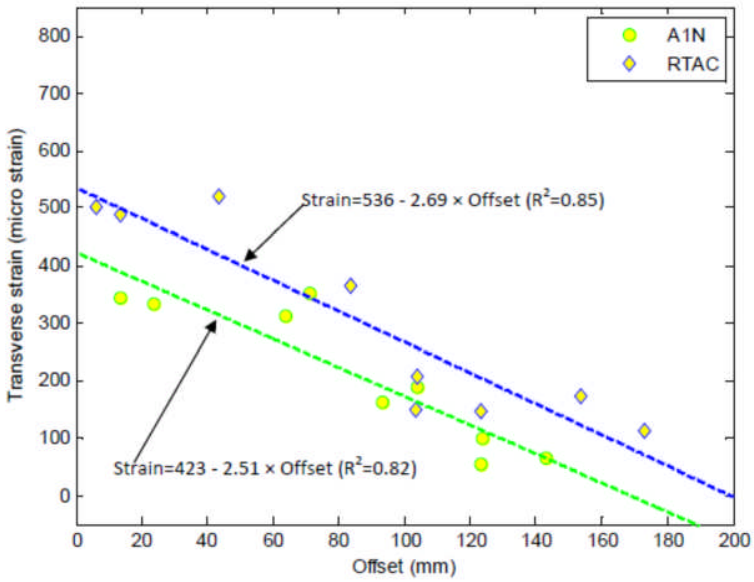

Figure 3 Relationship between measured transverse strains and offset under various loads at 345 kPa.

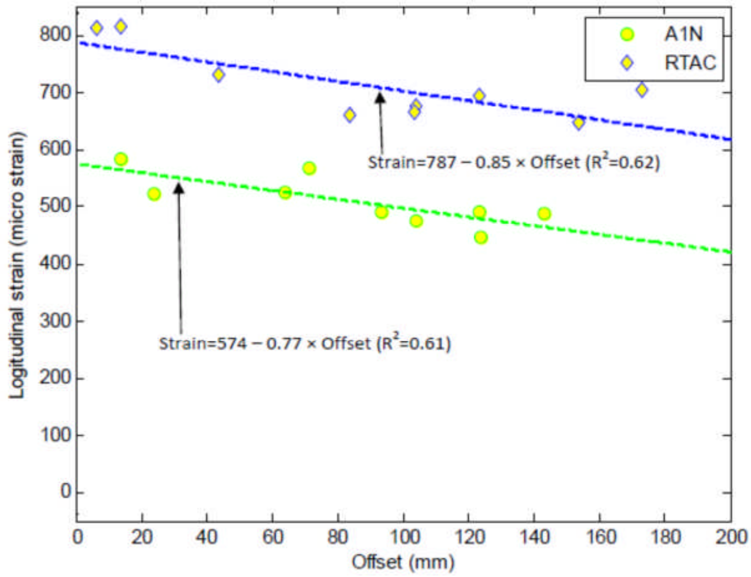

Figure 4 Relationship between measured longitudinal strains and offset under various loads at 345 kPa.

Table 3 shows the regression parameters for field test at 20km/h, 345 kPa for tire pressures, and two load levels. The absolute values of β for transverse strains were greater than the corresponding values of longitudinal strains. This steeper slope indicates that the transverse strains were more sensitive to the tire offset than the longitudinal strains. This observation agrees with the findings of Willis and Timm (4). This may be due to the time of loading on the gauge and the capture rate of the sensor. For the transverse gauge, the tire traveled perpendicular to the gauge and produced a short wave form and resulting shorter loading time. The shorter load time resulted in lower strains. For the gauge in the longitudinal direction, the tire traveled parallel to the gauge and produced a longer wave form and resulting longer loading time. The longer load time produced higher strains at the same offset as the transverse gauge.

Table 3 Regression Parameters for Field Tests

Strain orientation	Load rating	β	R^2	F-statistic	P-value	F-test
Transverse	A1N	-2.51	0.82	32.4227	0.0007	pass
	RTAC	-2.69	0.85	38.7888	0.0004	pass
Longitudinal	A1N	-0.77	0.61	10.9914	0.0128	pass
	RTAC	-0.85	0.62	11.2965	0.0121	pass

An F-test statistical analysis was conducted at the 95% confidence level to determine the significance of the linear regression parameters at the null-hypothesis. If the F-statistic is greater than the confidence level F-critical, it can be concluded that the model parameters were statistically significant from zero (i.e. null hypothesis) and could be used to predict the normalized strain.

Similar analyses were carried out for various combinations of tire pressure, load level, truck speed, and tire groups. Table 4 shows the normalized maximum strain and the difference (%) when tire pressure deflated from 690 kPa to 345 kPa with various loads. In most cases, the normalized tensile strain decreased significantly.

Table 4 Normalized Strain and the Differences between 690 kPa and 345 kPa at Various Loads

Load rating	Gauge Orientation	Drive			Trailer1			Trailer2		
		ε_{690} (10^{-6})	ε_{345} (10^{-6})	% Difference	ε_{690} (10^{-6})	ε_{345} (10^{-6})	% Difference	ε_{690} (10^{-6})	ε_{345} (10^{-6})	% Difference
A1N	Transverse	775	530	-32	586	472	-20	623	422	-32
	Longitudinal		621			574			598	
RTAC	Transverse	586	638	9	579	589	2	615	579	-6
	Longitudinal	941	827	-12	869	777	-11	948	850	-10

3. FINITE ELEMENT SIMULATION

Kim and Tutumluer (5) found that the domain size of 140-times the radius of circular loading area (R) in the vertical direction and 20-times R in the horizontal direction gives more accurate results using the 8-node isoparametric quadrilateral elements. Al-Qadi et al (6) found that the horizontal location of the infinite boundary from the load center needs to be greater than 900 mm in order to have the closest solution to the full-size reference FE model. The location of the bottom infinite boundary element was recommended at a depth of 1100 mm, where the maximum compressive stress in the subgrade became insignificant at 1% or less of the maximum tire-pavement contact stress. Witczak et al (7) suggested the infinite boundaries at 760 to 2000 mm. Park (8) found that a finite element mesh with lateral and longitudinal dimensions of 3810 mm x 3810 mm was appropriate with infinite elements in depth. In their study, Wang and Machemehl (9) found a pavement structure solid having X, Y, and Z of 4000 mm x 4000 mm x 6000 mm is accurate enough to validate roller boundary conditions.

As shown in Figure 5, a pavement block with X, Y, and Z of 2200 mm X 4400 mm x 6000 mm was used to compute the pavement responses for dual tire tandem axle configuration. Good interface bonding was assumed for different layers. The eight-node, linear brick elements with ABAQUS were used for 3-dimension finite elements analysis.

A finer FE mesh was placed under the loaded area where the change in strain is greatest and increasingly coarser mesh was employed away from the load where the change in strain is slower. The element dimension of the finer mesh was chosen equal to the size of footprint sensing area which is 8.38 mm for both longitudinal and transverse directions. Tire and pavement contact pressure was inputted to the FE modeling as can be seen in Figure 6.

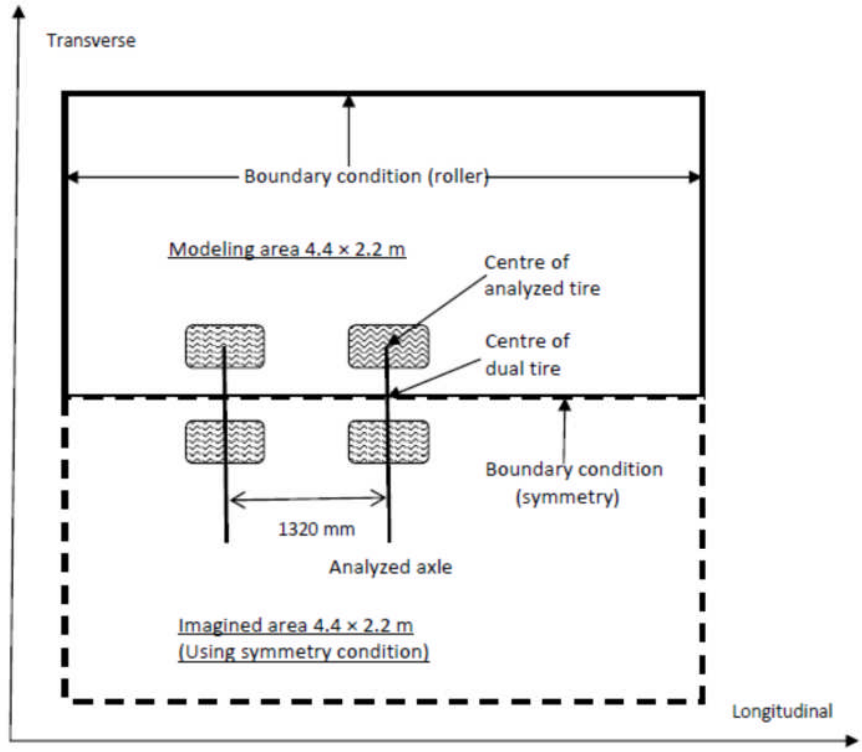

Figure 5 Plan view of FE modeling area for dual tire tandem axle

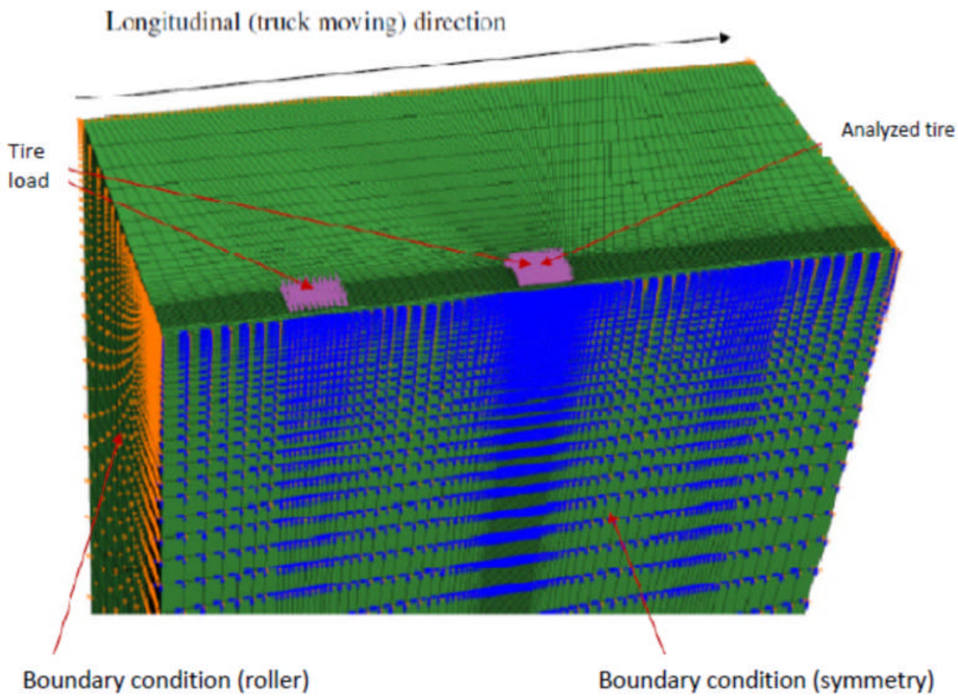

Figure 6 Load and boundary conditions of FE modeling

3.1 Distribution of Simulated Strains

The strains of the pavement at different locations were simulated for various combinations of tire load, tire pressure, and truck speed. Figure 7 through figure 9 show the distribution of horizontal strains at the bottom of AC layer and vertical strain on the top of subgrade under A1N load.

As can be seen from Figure 7, the maximum strain decreased by 15.2% from 112 to 95 micro strains under the centre of the analyzed tire when tire pressure deflated from 690 kPa to 345 kPa. The maximum transverse strain is under the centre of analyzed tire. From the centre of the analyzed tire to the centre of the dual tire(the distance is 165.9 mm), the transverse strain decreased from 112 to 19 micro strains (tire pressure 690 kPa), which gives the reason why the measured transverse strain by strain gauges is so sensitive to wheel offset of test truck (10).

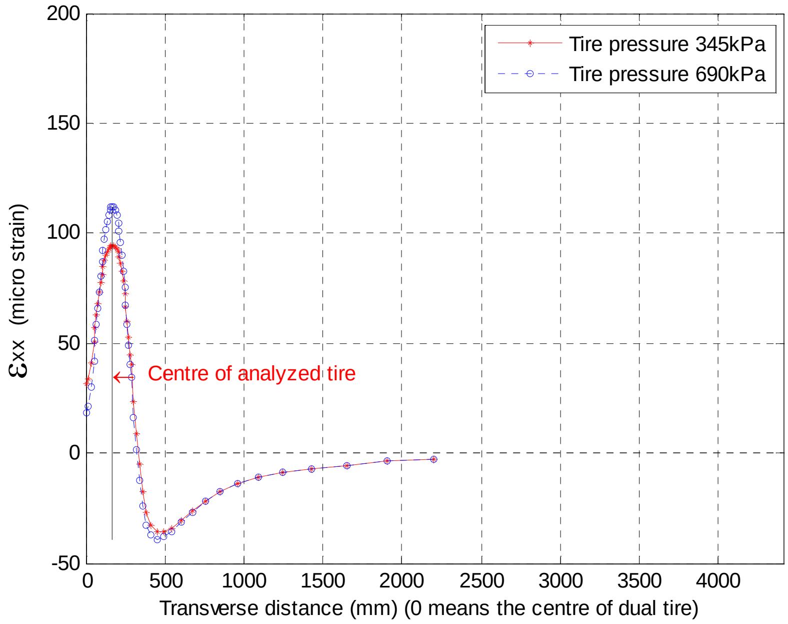

Figure 7 Transverse strains at bottom of AC layer along transverse direction under the centre of analyzing tire with A1N load

Figure 8 shows the distribution of longitudinal strain at bottom of AC layer along transverse direction under the centre of analyzed tire with A1N load. The maximum longitudinal strain decreased by 16.1% from 180 to 151 micro strains when tire pressure deflated from 690 kPa to 345 kPa. The maximum longitudinal strain is not produced under the centre of the analyzed tire. The maximum strain is produced somewhere between the centre of dual tire assembly and the centre of analyzed tire depending on tire pressure. For example, the maximum longitudinal strain (180 micro strains) is 50 mm away from the centre of analyzed tire toward the centre of dual tire at tire pressure of 690 kPa. This observation shows the effect of strain overlap of the dual tires.

The longitudinal strain at the bottom of AC layer does not change much from the centre of analyzed tire to the center of the dual tires. The strain is 120 micro strains under the centre of analyzed tire; the corresponding value is 121 micro strains under the centre of dual tire at tire pressure of 690 kPa. This gives the reason why longitudinal strain gauges always captured much better readings than transverse strain gauges during the field test (10).

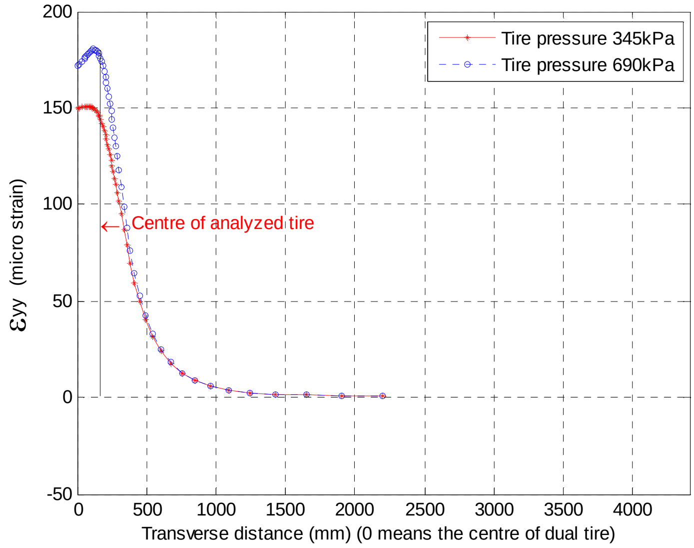

Figure 8 Longitudinal strains at bottom of AC layer along transverse direction under the centre of analyzed tire with A1N load

Figure 9 shows the distribution of vertical strains on top of subgrade along transverse direction. The maximum vertical strain on top of subgrade is under the centre of the dual tires because of the effect of strain overlap of the two tires of each axle. The vertical strain on top of the subgrade decreased only 1.8% when tire pressure deflated from 690 kPa to 345 kPa. This indicates that the vertical compressive strain on top of subgrade is dominated by the tire group load instead of the distribution of the contact pressure.

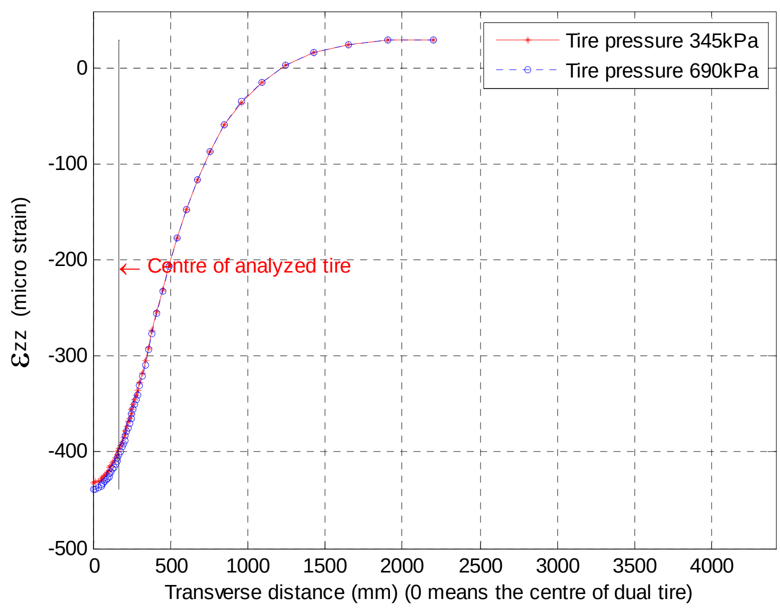

Figure 9 Vertical strains on top of subgrade along transverse direction under the centre of analyzed tire with A1N load

3.2 Summary of Computed Strains

Table 5 shows the simulated pavement responses at the bottom of AC layer or on top of the subgrade under various loads. When tire pressure deflated from 690 kPa to 345 kPa, the tensile strain at the bottom of AC layer decreased in average by 16.5% which is compatible to the filed data. The compression strain on top of the subgrade decreased only 1.7% in average. These results may indicate that reduced tire pressure is effective to prevent bottom up failure of AC layer, but may not be effective to prevent pavement rutting.

Table 5 Simulated pavement responses at the bottom of AC layer and on top of the subgrade under various loads and tire pressure

Load rating	Gauge Orientation	Drive			Trailer1			Trailer2		
		ε_{690} (10^{-6})	ε_{345} (10^{-6})	% Difference	ε_{690} (10^{-6})	ε_{345} (10^{-6})	% Difference	ε_{690} (10^{-6})	ε_{345} (10^{-6})	% Difference
A1N	Transverse	112	95	-15.2	120	107	-10.8	123	109	-11.4
	Longitudinal	180	151	-16.1	167	150	-10.2	183	162	-11.5
	Vertical	-439	-432	-1.6	-390	-386	-1.0	-436	-433	-0.7
RTAC	Transverse	127	106	-16.5	143	125	-12.6	124	111	-10.5
	Longitudinal	205	168	-18.1	202	177	-12.4	193	172	-10.9
	Vertical	-495	-486	-1.8	-458	-452	-1.3	-457	-452	-1.1

3.3 Test FE Results against Field Data

By comparing normalized measured strain in Table 4 with simulated pavement responses in Table 5, in average, a factor of 4.5 can be applied to the simulated strains by FE model, There are mainly four sources of the variability for the measured strains: wheel wander, the precision of the gauge themselves, material variability, and the gauge alignment (11). For this research, the following two features may lead to the factor greater than one: the test section is aged pavement; the strain gauges were installed by using cold mix and compacted manually; the moduli for FE modeling are back calculated from FWD test which may be subject to some error.

4. CONCLUSIONS

Base on the results and discussions in this paper, the following conclusions can be drawn:

- Reduced tire inflation pressure is effective to reduce tensile strain at the bottom of asphalt pavement, but not helpful to reduce the compression strain on top of the subgrade. These observations may indicate that TPCS may be helpful to prevent bottom up failure of AC layer, but may not be effective to prevent pavement rutting.
- The decrease of measured strains agrees with the increase of footprint area when tire pressure deflated.
- The measured value of tensile strain at the bottom of AC layer is compatible with simulated strains by FE model. A factor of 4.5 can be applied.
- The simulated tensile strain at the bottom of AC layer decreases 15% in average when tire pressure deflated from 690 kPa to 345 kPa for various loads and axles. This value is compatible to and normalized measured values of TPCS tests.
- Transverse strain is more sensitive than longitudinal strain to the transverse distance to the centre of analyzed tire.

5. ACKNOWLEDGEMENTS

The authors acknowledge the contributions of Pinnovations-FERIC Division, Manitoba Infrastructure and Transportation, and Manitoba Conservation for funding this research.

REFERENCES

1. Stuart III, E., Gililland, E., and Della-Moretta, L. (1987). The Use of Central Tire Inflation Systems on Low-volume Roads. *Transportation Research Record N1106, Fourth International Conference on Low-Volume Roads, Volum4 1.* (pp. 164-168). Transportation Research Board.
2. Bradley, A. (2006). Hauling with Full axle Weights and Reduced Tire Pressure on Weight-Restricted Roads in British Columbia. *Transportation Research Record: Journal of the Transportatin Research Board (No. 1967)* , 20-26. Washington D.C.: Transportation Research Board of the National Academies.
3. Timm, D. and A. Priest, A. (2005). *Wheel Wander at the NCAT Test Track*. Publication NCAT Report 05-02. National Center for asphalt Technology, Auburn University, 2005.
4. Willis, J., and Timm, D. (2008). Repeatability of Asphalt Strain measurement Under Full-Scale Dynamic Loading. In *Transportation Research Record: Journal of the Transportation Reserach Board*, No. 2087, Transportation Research Board of the National Academies, Washington, D.C., 2008, pp. 40-48.
5. Kim, M. and Tutumluer, E. (2007). Nonlinear Pavement Foundation Modeling for Three-Dimensional Finite Element Analysis of Flexible Pavements. *TRB2007 Annual Meeting CD-ROM.*
6. Al-Qadi, I., Wang, H. and Yoo, P. (2008). Dynamic Analysis and In-Situ Validation of Perpetual Pavement Response to Vehicular Loading. *TRB 2008 Annual Meeting CD-ROM.*
7. Witczak, M., Schwartz, C., Feng, Y., Uzan, J., and Mirza, W. (2004). Finite element Procedures for Flexible Pavement Analysis. *NCHRP Finial Document, Appendix RR* . Washington D.C.: Transportation Research Board.
8. Park, D. (2008). Prediction f Pavement Fatigue and Rutting Life Using Different Tire Types. *KSCE Journal of Civil Engineering* , 297-303.
9. Wang, F. and Machemehl, R. (2006). *Predicting Truck Tire Pressure Effects upon Pavement Performance.* Texas: Center for Transportation Research, University of Texas at Austin.
10. Liu, Q., kavanagh, L., and Shalaby, A. (2010). Instrumented Pavement Response under Standard and Reduced Tire Pressure. Halifax: Transportation Association of Canada.
11. Timm, J. (2008). Repeatability of Asphalt Strain measurement Under Full-Scale Dynamic Loading. *Transportation Research Record: Journal of the Transortation Research Board (No. 2087)* , 40-48. Washington D.C.: Transpotation Research Board of the National Academies.